

1  
2  
3  
4  
5  
6  
7  
8  
9  
10  
11  
12  
13  
14  
15  
16  
17  
18  
19  
20  
21  
22  
23  
24  
25  
26  
27  
28  
29  
30  
31  
32  
33  
34  
35  
36  
37  
38  
39  
40  
41  
42  
43  
44  
45  
46  
47  
48  
49  
50  
51  
52  
53  
54  
55  
56  
57  
58  
59  
60  
61  
62  
63  
64  
65

1 **Estimation of global soil respiration by accounting for land-use changes derived**  
2 **from remote sensing data**

4 Minaco ADACHI<sup>1,5,\*</sup>, Akihiko ITO<sup>2</sup>, Seiichiro YONEMURA<sup>3</sup>, Wataru TAKEUCHI<sup>4</sup>

6 <sup>1</sup> Institute of Industrial Science, the University of Tokyo, 4-6-1 Komaba, Meguro-ku,  
7 Tokyo 153-8505, Japan

8 <sup>2</sup> National Institute for Environmental Studies, 16-2 Onogawa, Tsukuba, Ibaraki  
9 305-8506, Japan, itoh@nies.go.jp

10 <sup>3</sup> National Institute for Agro-Environmental Studies, NARO, 3-1-3 Kannondai, Tsukuba,  
11 Ibaraki 305-8604, Japan, yone@affrc.go.jp

12 <sup>4</sup> Institute of Industrial Science, the University of Tokyo, 4-6-1 Komaba, Meguro-ku,  
13 Tokyo 153-8505, Japan, wataru@iis.u-tokyo.ac.jp

14 <sup>5</sup> Graduate school of Life and Environmental Science, the University of Tsukuba, 1-1-1  
15 Tennodai, Tsukuba, Ibaraki 305-8577, Japan, adachi.minaco.gf@u.tsukuba.ac.jp

17 \* Corresponding author: Minaco ADACHI  
18 Graduate school of Life and Environmental Science,  
19 The University of Tsukuba, 1-1-1 Tennodai, Tsukuba, Ibaraki 305-8577, Japan  
20 Tel. &Fax: +81-29-853-8857  
21 E-mail: adachi.minaco.gf@u.tsukuba.ac.jp

**Highlights:**

- We estimated the global soil respiration using empirical equations based on field observation and climate data and land-use maps obtained via remote sensing.
- The global soil respiration was estimated to be 94.8 and 93.8 Pg C yr<sup>-1</sup> in 2001 and 2009, respectively.
- The spatial variation of soil respiration ( $Q_{10}$ ) values was higher but its spatial variation was lower in high-latitude areas than in other areas.
- Due to the high uncertainties in the input data and equations used in our analysis, it will be necessary to develop more accurate estimates of global soil respiration.

1  
2 **23 Abstract**  
3  
4

5  
6 24 Soil respiration is one of the largest carbon fluxes from terrestrial ecosystems. Estimating  
7  
8  
9 25 global soil respiration is difficult because of its high spatiotemporal variability and  
10  
11  
12 26 sensitivity to land-use change. Satellite monitoring provides useful data for estimating the  
13  
14  
15  
16 27 global carbon budget, but few studies have estimated global soil respiration using satellite  
17  
18  
19 28 data. We provide preliminary insights into the estimation of global soil respiration in  
20  
21  
22  
23 29 2001 and 2009 using empirically derived soil temperature equations for 17 ecosystems  
24  
25  
26  
27 30 obtained by field studies, as well as MODIS climate data and land-use maps at a 4-km  
28  
29  
30  
31 31 resolution. The daytime surface temperature from winter to early summer based on the  
32  
33  
34 32 MODIS data tended to be higher than the field-observed soil temperatures in subarctic  
35  
36  
37 33 and temperate ecosystems. The estimated global soil respiration was 94.8 and 93.8 Pg C  
38  
39  
40  
41 34 yr<sup>-1</sup> in 2001 and 2009, respectively. However, the MODIS land-use maps had insufficient  
42  
43  
44 35 spatial resolution to evaluate the effect of land-use change on soil respiration. The spatial  
45  
46  
47  
48 36 variation of soil respiration ( $Q_{10}$ ) values was higher but its spatial variation was lower in  
49  
50  
51 37 high-latitude areas than in other areas. However,  $Q_{10}$  in tropical areas was more variable  
52  
53  
54  
55 38 and was not accurately estimated (the values were >7.5 or <1.0) because of the low  
56  
57  
58  
59 39 seasonal variation in soil respiration in tropical ecosystems. To solve these problems, it  
60  
61  
62  
63  
64  
65

1  
2  
3  
4  
5  
6  
7  
8  
9  
10  
11  
12  
13  
14  
15  
16  
17  
18  
19  
20  
21  
22  
23  
24  
25  
26  
27  
28  
29  
30  
31  
32  
33  
34  
35  
36  
37  
38  
39  
40  
41  
42  
43  
44  
45  
46  
47  
48  
49  
50  
51  
52  
53  
54  
55  
56  
57  
58  
59  
60  
61  
62  
63  
64  
65

40 will be necessary to validate our results using a combination of remote sensing data at  
41 higher spatial resolution and field observations for many different ecosystems, and it will  
42 be necessary to account for the effects of more soil factors in the predictive equations.

43

44 **Keywords:** soil temperature, MODIS, land-use change

45

46

1  
2 **47 1. Introduction**  
3  
4

5  
6 48 Soil is a major carbon (C) reserve in terrestrial ecosystems. Soil respiration ( $R_s$ ) is a large  
7  
8  
9 49 carbon flux from terrestrial ecosystems to the atmosphere.  $R_s$  is related to the amount of  
10  
11  
12 50 soil carbon input, soil carbon stocks, root biomass, microbial biomass, temperature, and  
13  
14  
15  
16 51 soil water content (Davidson and Janssens, 2006; Sato et al., 2015). Soil organic carbon  
17  
18  
19 52 (SOC) dynamics at global scales, which include  $R_s$ , have many uncertainties, and the  
20  
21  
22  
23 53 estimation of global  $R_s$  is difficult because of high spatiotemporal variability (Smith and  
24  
25  
26  
27 54 Fang, 2010). As a result, estimates of global  $R_s$  have varied widely, ranging from 68 PgC  
28  
29  
30 55  $\text{yr}^{-1}$  (Raich and Schlesinger, 1992) to 98 PgC  $\text{yr}^{-1}$  (Bond-Lamberty and Thomson, 2010).  
31  
32  
33  
34 56 Soil temperature is the main factor that influences soil carbon dynamics (Carvalhais et al.,  
35  
36  
37 57 2014; Davidson and Janssens, 2006), including  $R_s$  (Bond-Lamberty and Thomson, 2010;  
38  
39  
40  
41 58 Raich and Schlesinger, 1992; Reichstein and Beer, 2008; Zhou et al., 2009). In one study,  
42  
43  
44 59 the temperature sensitivity of  $R_s$  per 10° C change in temperature (i.e.,  $Q_{10}$ ) at a global  
45  
46  
47  
48 60 scale varied from 1.43 to 2.03 among ecosystems (Zhou et al., 2009), but in another, the  
49  
50  
51  
52 61 mean global  $Q_{10}$  was lower, at 1.4 (Hashimoto et al., 2015). In other cases, low soil water  
53  
54  
55 62 content decreased  $R_s$  of a savanna landscape under extremely dry conditions (Chen et al.,  
56  
57  
58  
59 63 2002), whereas a decrease in the depth to ground water decreased  $R_s$  in a tropical swamp  
60  
61  
62  
63  
64  
65

1  
2 64 forest (Hirano et al., 2014). As a result, some models of  $R_s$  also include a soil moisture  
3  
4  
5 65 term (e.g., Sotta et al., 2004).  
6  
7

8  
9 66 Land-use change also affects the SOC content since the accumulation rates of soil  
10  
11  
12 67 carbon change in response to changes in the input rates of organic matter, in  
13  
14  
15  
16 68 decomposition rates, and in physical and biological conditions in the soil that result from  
17  
18  
19 69 land-use changes (Post and Kwon, 2000). According to a meta-analysis by Guo and  
20  
21  
22  
23 70 Gifford (2002), the conversion of natural forest or pasture into cropland decreases soil  
24  
25  
26  
27 71 carbon stocks. Therefore, estimates of global  $R_s$  should account for changes in land use  
28  
29  
30 72 and the differences in  $R_s$  among ecosystem types.  
31  
32

33  
34 73 Satellite monitoring provides not only land cover maps but also useful vegetation  
35  
36  
37 74 and environmental data that can be used to estimate the global carbon budget in terrestrial  
38  
39  
40  
41 75 ecosystems, and especially the carbon exchange between the atmosphere and ecosystems,  
42  
43  
44 76 because it permits estimates of the land surface temperature, gross primary production  
45  
46  
47  
48 77 (GPP), net primary production (NPP), and leaf area index (Guo et al., 2012). For instance,  
49  
50  
51 78 these datasets from the Moderate Resolution Imaging Spectroradiometer (MODIS) have  
52  
53  
54  
55 79 been used as inputs for carbon cycling models (e.g., Ise et al., 2010; Sasai et al., 2005,  
56  
57  
58 80 2011; Yuan et al., 2015).  
59  
60  
61  
62  
63  
64  
65

1  
2 81 It is important to understand both the overall CO<sub>2</sub> budget of terrestrial ecosystems and the  
3  
4  
5  
6 82 CO<sub>2</sub> dynamics in each compartment (e.g., plants versus soil). Although remote sensing  
7  
8  
9 83 cannot directly observe  $R_s$ , long-term and global  $R_s$  can be estimated based on the values  
10  
11  
12 84 of environmental factors (such as surface temperatures) that control  $R_s$  and that can be  
13  
14  
15  
16 85 observed by remote sensing. Estimates of global  $R_s$  will provide accuracy comparable to  
17  
18  
19 86 that of other satellite data (e.g., data from the Greenhouse gases observing satellite;  
20  
21  
22  
23 87 Yokota et al., 2009) and can be used to improve our understanding of the sources of  
24  
25  
26  
27 88 changes in carbon cycling from ecosystems. However, no studies have evaluated the  
28  
29  
30  
31 89 effect of land-use change on global  $R_s$  using MODIS remote sensing data.  
32  
33

34 90 In the present study, we provide preliminary insights into the estimation of global  $R_s$   
35  
36  
37 91 by combining empirical equations derived from field studies with satellite data (climate  
38  
39  
40  
41 92 and land cover). Our objectives were to (1) obtain soil temperature data using MODIS  
42  
43  
44 93 land surface temperature data, (2) identify the variation in global  $R_s$  and  $Q_{10}$  from 2001 to  
45  
46  
47  
48 94 2009, and (3) discuss the effects of land-use change on global  $R_s$ .  
49  
50

51 95

## 52 96 **2. Materials and methods**

### 53 97 *2.1. MODIS data*

1  
2  
3  
4  
5  
6  
7  
8  
9  
10  
11  
12  
13  
14  
15  
16  
17  
18  
19  
20  
21  
22  
23  
24  
25  
26  
27  
28  
29  
30  
31  
32  
33  
34  
35  
36  
37  
38  
39  
40  
41  
42  
43  
44  
45  
46  
47  
48  
49  
50  
51  
52  
53  
54  
55  
56  
57  
58  
59  
60  
61  
62  
63  
64  
65

98 Daily MODIS land surface temperatures during the day and night ( $LST_d$  and  $LST_n$ ,  
99 respectively) were calculated by interpolation using some remote sensing products (e.g.,  
100 the 8-day composite LST at a 4-km spatial resolution from the MOD11C3 product, and  
101 vegetation data at a 10-m resolution from the AVNIR2 product). This approach was  
102 necessary because data with high spatial resolution may not cover sufficiently large areas  
103 for a given study (Takeuchi et al., 2012), as was the case in the present global-scale study.  
104 When vegetation was present,  $LST_d$  and  $LST_n$  were estimated above the vegetation. Soil  
105 water content (SWC) was estimated using the modified Keetch-Byram drought index  
106 (KBDI) based on remote sensing data (Keetch and Byram, 1968; Takeuchi et al., 2010),  
107 as follows:

108

$$109 \quad SWC = SWC_{max} [1 - (KBDI / 800)] \quad (1)$$

110

111 where  $SWC_{max}$  is the maximum soil water content at each study site based on published  
112 data, but most  $R_s$  equations do not include SWC parameters (summarized in Table S1 of  
113 the supporting information). Land cover was distinguished for the 17 ecosystem types in  
114 the table using the MODIS MOD12Q1 product (collection 5) at a 4-km spatial resolution.

1  
2 115 This classification scheme was developed by the International Geosphere–Biosphere  
3  
4  
5 116 Programme Data and Information Systems initiative (Friedl et al., 2002). This land cover  
6  
7  
8  
9 117 map did not detect the paddy field and tundra classes. Each point in the land cover map  
10  
11  
12  
13 118 from the MOD12Q1 product was assigned to one of the 17 ecosystem classes.  
14  
15

16 119

## 20 120 *2.2. Validation of MODIS surface temperatures using field observation*

21  
22  
23 121  $R_s$  in this study was predominantly estimated as a function of soil temperature (Table S1).  
24

25  
26 122 We compared the MODIS estimates ( $LST_d$  and  $LST_n$ ) to empirical data based on field  
27  
28

29 123 observations (daily mean air temperature and soil temperature) at five sites: an evergreen  
30  
31

32  
33  
34 124 needleleaf forest in Alaska (64°52'N, 147°51'W; Ueyama et al., 2014), a mixed forest in  
35

36  
37 125 Japan (36°08'N, 137°25'E; from the AsiaFlux database, <http://asiaflux.net>), cropland in  
38  
39

40  
41 126 Japan (36°01'N, 140°07'E; Kishimoto-Mo et al., unpublished data), an evergreen  
42  
43

44 127 broadleaf forest in Thailand (14°29'N, 101°54'E, AsiaFlux database), and an evergreen  
45  
46

47  
48 128 broadleaf forest in Malaysia (2°58'N, 102°18'E, AsiaFlux database). The measurement  
49  
50

51 129 height for air temperature and the depth of the soil temperature measurement differed  
52  
53

54  
55 130 among the five sites, with respective values of 800 cm and –10 cm in the evergreen  
56  
57

58  
59 131 needleleaf forest, 1800 cm and –1 cm in the mixed forest, 200 cm and –2 cm in the  
60  
61

1  
2 132 cropland, 4500 cm and -5 cm in the evergreen broadleaf forest in Thailand, and 5300 cm  
3  
4  
5 133 and -2 cm in the evergreen broadleaf forest in Malaysia. We could not quantify the effects  
6  
7  
8  
9 134 of these different measurement heights on estimation of  $R_s$  in each ecosystem because  
10  
11  
12 135  $LST_d$  and  $LST_n$  were measured at the top of the dominant vegetation, and that height  
13  
14  
15  
16 136 varied with the type of vegetation.  
17

18  
19  
20 137 Table S1 provides the empirical equations for estimating  $R_s$  in the 17 ecosystems  
21  
22  
23 138 from around the world. We selected empirical equations that were based on field  
24  
25  
26  
27 139 measurements (not data obtained using incubation or manipulation experiments)  
28  
29  
30 140 conducted since 2000 from version 3.0 of a global  $R_s$  database (Bond-Lamberty and  
31  
32  
33  
34 141 Thomson, 2014). Daily  $R_s$  values were estimated using the empirical  $R_s$  equation  
35  
36  
37  
38 142 corresponding to the land use type for each pixel, the estimated soil temperature, and the  
39  
40  
41 143 soil water content in each pixel of the grid (Fig. 1).  $R_s$  in the evergreen broadleaf forest,  
42  
43  
44 144 which is mainly a tropical forest, was estimated using only the soil water content when  
45  
46  
47  
48 145 land surface temperature (LST) was  $>25^\circ\text{C}$  (Sotta et al., 2004). In addition, LST of  
49  
50  
51  
52 146 grassland vegetation areas were sometimes more than  $30^\circ\text{C}$ , and if we calculated  $R_s$  using  
53  
54  
55 147 an exponential function, the estimated  $R_s$  was unrealistically high in these areas. Richards  
56  
57  
58  
59 148 et al. (2012) reported that  $R_s$  in a savanna decreased when the soil temperature was over  
60  
61  
62  
63  
64  
65

1  
2 149 30°C. Thus, if the LST for a savanna pixel was >30°C, we recalculated LST to be less  
3  
4  
5  
6 150 than 26°C for the estimation of  $R_s$  in the ecosystems that included savanna vegetation  
7  
8  
9 151 (closed and open shrubland, grassland, savanna, woody savanna, grassland, cropland, and  
10  
11  
12  
13 152 cropland–natural vegetation mosaic).

14  
15  
16 153 We modelled the dependency of  $R_s$  on temperature at a global scale according to the  
17  
18  
19  
20 154 following relationship:

21  
22  
23 155

$$24  
25  
26 156 \quad R_{s\_est} = \alpha \times e^{\beta T} \quad (2)$$

27  
28  
29  
30 157

31  
32  
33  
34 158 where  $R_{s\_est}$  is the estimated daily  $R_s$  in this study,  $T$  is the  $LST_d$  at each point (4-km  
35  
36  
37  
38 159 resolution), and  $\alpha$  and  $\beta$  are fitting parameters. We calculated  $R_{s\_est}$  using the least-squares  
39  
40  
41 160 method based on  $R_s$  (Table S1) and  $LST_d$  over 365 days at a 4-km resolution. We  
42  
43  
44  
45 161 calculated the  $Q_{10}$  of  $R_s$  as follows:

46  
47  
48 162

$$49  
50  
51 163 \quad Q_{10} = e^{10\beta} \quad (3)$$

52  
53  
54  
55 164

56  
57  
58 165 *2.3. Statistical analyses*

1  
2 166 Statistical analyses were performed using version 3.3.1 of the R software (R  
3  
4  
5 167 Development Core Team, 2016). Pearson's product-moment correlation coefficient was  
6  
7  
8  
9 168 used to clarify relations between  $LST_n$  values and soil temperature based on field data  
10  
11  
12  
13 169 from the evergreen needleleaf forest, mixed forest, and cropland areas (Fig. 3).  
14  
15

16 170

### 171 **3. Results**

#### 172 *3.1. Estimation of soil temperature*

173 We compared  $LST_d$  and  $LST_n$  in the five ecosystems with the observed daily mean air and  
174 soil temperatures in the field (Fig. 2). At the Alaska and Japan sites, the observed soil  
175 temperatures from winter to early summer were lower than the  $LST_d$  (Fig. 2a-c).  $LST_n$   
176 values in these ecosystems were significantly correlated with the soil temperature from  
177 winter to early summer (Fig. 3,  $P < 0.001$ ). We estimated soil temperatures during the  
178 winter to early summer for subarctic and temperate areas using the equations in Figure 3,  
179 which used  $LST_n$  to calculate  $R_s$  in six of the ecosystems: evergreen needleleaf forest,  
180 deciduous needleleaf forest, deciduous broadleaf forest, mixed forest, cropland, and the  
181 cropland–natural vegetation mosaic. In the tropical regions,  $LST_d$  was generally lower  
182 than the actual air temperature in the evergreen broadleaf forests in Thailand (Fig. 2d).

1  
2  
3  
4  
5  
6  
7  
8  
9  
10  
11  
12  
13  
14  
15  
16  
17  
18  
19  
20  
21  
22  
23  
24  
25  
26  
27  
28  
29  
30  
31  
32  
33  
34  
35  
36  
37  
38  
39  
40  
41  
42  
43  
44  
45  
46  
47  
48  
49  
50  
51  
52  
53  
54  
55  
56  
57  
58  
59  
60  
61  
62  
63  
64  
65

183

184 *3.2. Land-use change*

185 To quantify the magnitude of land-use change, we counted the number of pixels for each  
ecosystem type based on the MODIS land cover maps in 2001 and 2009 and used these  
186 sums to calculate the percentage of the total area occupied by each ecosystem (Table S2).  
187  
188 The cropland and cropland–natural vegetation mosaic types accounted for approximately  
189 10% of the world’s land area in both years, but the cropland–natural vegetation mosaic  
190 decreased from 4.0% of the total land area in 2001 to 3.6% in 2009. The total forest area  
191 (evergreen needleleaf forest, evergreen broadleaf forest, deciduous needleleaf forest,  
192 deciduous broadleaf forest, and mixed forest) increased from 14.1% in 2001 to 15.3% in  
193 2009. In particular, the areas of evergreen needleleaf forests in North America and Russia  
194 and of the deciduous needleleaf forest in northern Russia increased. The areas of  
195 grassland and woody savanna both decreased from 2001 to 2009.

196

197 *3.3. Estimation of global  $R_s$  and  $Q_{10}$*

198 We estimated annual global  $R_s$  values of 94.8 and 93.8 Pg C yr<sup>-1</sup> in 2001 and 2009,  
199 respectively; Figure 4 shows the regional distribution of the components of these total

1  
2 200 values. The mean annual  $R_s$  in each ecosystem except urban and built-up land, snow and  
3  
4  
5 201 ice, and tundra (for which  $R_s$  was assumed to equal 0) ranged from 77 to 1030  $\text{gC m}^{-2} \text{yr}^{-1}$   
6  
7  
8  
9 202 in 2001 (Fig. 5). The decrease in global annual  $R_s$  from 2001 to 2009 was mainly caused  
10  
11  
12 203 by decreases in the areas of woody savanna, deciduous broadleaf forest, and the  
13  
14  
15 204 cropland–natural vegetation mosaic (Table S2). The spatial variation of the  $Q_{10}$  values  
16  
17  
18 205 was higher but its spatial variation was lower in high-latitude areas than in other areas  
19  
20  
21 206 (Fig. 6). However,  $Q_{10}$  values in tropical areas could not be accurately estimated (the  
22  
23  
24 207 values were  $>7.5$  or  $<1.0$ ) because of low seasonal variation in  $R_s$  in the tropical  
25  
26  
27 208 ecosystems (mainly evergreen broadleaf forest, savanna, and woody savanna). In  
28  
29  
30  
31 209 addition, areas with low  $Q_{10}$  values in North America and Eurasia were mainly urban and  
32  
33  
34  
35 210 built-up areas.  
36  
37  
38  
39  
40  
41  
42  
43  
44

#### 45 212 **4. Discussion**

46  
47  
48 213 Both the  $LST_d$  and the  $LST_n$  values based on MODIS data for the three ecosystems with  
49  
50  
51 214 field-observed temperature data were correlated with the observed daily mean air and soil  
52  
53  
54 215 temperatures, especially for the relationship between  $LST_n$  and soil temperature from  
55  
56  
57  
58 216 winter to early summer in the subarctic and temperate ecosystems (Fig. 3). On the other  
59  
60  
61  
62  
63  
64  
65

1  
2 217 hand,  $LST_d$  became similar to the autumn air and soil temperatures in the field for the  
3  
4  
5 218 evergreen needleleaf forest and mixed forest (Fig. 2a,b). These relationships would be  
6  
7  
8  
9 219 influenced by two important aspects of plant phenology: leaf flushing and litterfall.  
10  
11  
12 220 Satellite data are often used to monitor plant phenology (Linderholm, 2006), and a  
13  
14  
15  
16 221 combined analysis of satellite and eddy-covariance data showed that environmental  
17  
18  
19 222 conditions influenced the annual trends in GPP (Xia et al., 2015). Mao et al. (2012)  
20  
21  
22  
23 223 reported that the mean global GPP based on MODIS data was 111.58 PgC from 2000 to  
24  
25  
26  
27 224 2009, but they did not report seasonal trends, unlike in the present study. Beer et al.  
28  
29  
30 225 (2010) reported that global GPP was approximately 123 Pg C yr<sup>-1</sup> based on their  
31  
32  
33  
34 226 observations (eddy-covariance flux data and models). However, the relationships  
35  
36  
37 227 between  $R_s$  and GPP are not clear at an ecosystem scale, so we must integrate and  
38  
39  
40  
41 228 compare these components of the global terrestrial carbon cycle to more accurately  
42  
43  
44  
45 229 characterize the response of  $R_s$  to climate change and land use change.

46  
47  
48 230 The global  $R_s$  in the present study that we estimated using MODIS data at a 4-km  
49  
50  
51 231 resolution was similar to the results that have been estimated using field observation data:  
52  
53  
54  
55 232 98 Pg C yr<sup>-1</sup> in 2008 (Bond-Lamberty and Thomson, 2010), and 93.2 Pg C yr<sup>-1</sup> in 2001  
56  
57  
58  
59 233 and 92.7 Pg C yr<sup>-1</sup> in 2009 (Hashimoto et al., 2015). Some studies have reported that  
60  
61  
62  
63  
64  
65

1  
2 234 global  $R_s$  in the 2000s was greater than the values in the 1980s and 1990s  
3  
4  
5 235 (Bond-Lamberty and Thomson, 2010; Hashimoto et al., 2015). In the present study, the  
6  
7  
8  
9 236 mean annual  $R_s$  values for each ecosystem did not differ between 2001 and 2009 (Fig. 5).  
10  
11  
12 237 Because of a hiatus in global warming, the average global annual temperature did not rise  
13  
14  
15  
16 238 greatly between 1998 and 2012 (Kaufmann et al., 2011; Kosaka and Xie, 2013). On the  
17  
18  
19 239 other hand, our estimates of  $R_s$  did not show high spatial variation, even though field  
20  
21  
22  
23 240 observations indicated high spatial variation; for example, the annual  $R_s$  in temperate  
24  
25  
26 241 grassland ranged from 32 to 2800  $\text{gC m}^{-2} \text{yr}^{-1}$  (Bond-Lamberty and Thomson, 2014).  
27  
28  
29 242 Bond-Lamberty and Thomson (2010) showed that the annual  $R_s$  based on field  
30  
31  
32  
33 243 observations had high variation because the annual  $R_s$  of some temperate and tropical  
34  
35  
36  
37 244 biomes were greater than 2000  $\text{gC m}^{-2} \text{yr}^{-1}$ . We found higher spatial variation of the  $Q_{10}$   
38  
39  
40  
41 245 values in high-latitude areas than in other areas, but its spatial variation was lower and we  
42  
43  
44 246 could not reliably estimate  $Q_{10}$  values in the tropical areas (Fig. 6). Zhou et al. (2009)  
45  
46  
47  
48 247 reported that  $Q_{10}$  values were highest in tundra regions (2.03), whereas the  $Q_{10}$  of  
49  
50  
51 248 evergreen broadleaf forest (mainly in tropical regions) was only 1.50. Hashimoto et al.  
52  
53  
54  
55 249 (2015) also estimated that  $Q_{10}$  values in tropical regions were less than 1.5. Our results  
56  
57  
58  
59 250 suggested that  $LST_d$  in evergreen broadleaf forest showed low temporal variation (Fig.

1  
2 251 2e), and this would be one reason for uncertainty in the estimation of  $Q_{10}$  values in the  
3  
4  
5 252 tropical areas.  
6  
7

8  
9 253 We estimated the annual  $R_s$  using one empirical equation for each ecosystem;  
10

11  
12 254 however, it is unlikely that these equations remain sufficiently representative over large  
13  
14

15  
16 255 areas. To solve this issue, we need to validate the annual  $R_s$  and empirical equations using  
17  
18

19  
20 256 field observations from many different ecosystems. Moreover, we did not validate soil  
21  
22

23 257 water content using field observation data because we relied on previously published  
24  
25

26  
27 258 equations for  $R_s$  for all ecosystems, and most of the equations did not include soil water  
28  
29

30 259 content as a regression parameter. Some papers did not measure  $R_s$  during the winter or  
31  
32

33  
34 260 snowy season; for example, this was true for evergreen broadleaf forest (Pypker and  
35  
36

37 261 Fredeen, 2002) and larch forest (Jiang et al., 2005). Mo et al. (2005) suggested that  $R_s$   
38  
39

40 262 measured above a snow surface accounted for approximately 6 to 10% of the annual  $R_s$  in  
41  
42

43  
44 263 a cool temperate forest. Therefore, differences in the measurement period used to develop  
45  
46

47  
48 264 the empirical equations in Table S1 increased the uncertainty of our estimation of global  
49  
50

51 265  $R_s$ . Additionally, some studies reported that annual  $R_s$  changed in response to the age of  
52  
53

54  
55 266 vegetation (Saurette et al., 2006) and soil texture: clayey and sandy soils (Sugihara et al.,  
56  
57

58  
59 267 2012) and different management regimes (Richards et al., 2012; Yonemura et al., 2014)  
60  
61

1  
2 268 produced different results under the same climatic conditions. Janssens et al. (2010)  
3  
4  
5 269 reported an increase in nitrogen deposition from combustion of fossil fuels, and that this  
6  
7  
8  
9 270 fertilization decreased  $R_s$ . However, elevated atmospheric  $\text{CO}_2$  increased soil microbial  
10  
11  
12 271 activity and decomposition of soil organic matter, which would increase  $R_s$  (Carney et al.,  
13  
14  
15  
16 272 2007). Therefore, we need to consider these factors (e.g., the effect of land-use change,  
17  
18  
19 273 age of vegetation, soil texture, SOC, and nitrogen fertilization) when estimating  $R_s$  and  
20  
21  
22  
23 274 validate our results using field observations.  
24  
25

26  
27 275 The global  $R_s$  in the present study decreased by  $1.0 \text{ Pg C yr}^{-1}$  from 2001 to 2009, but  
28  
29  
30 276 we did not consider the net effect on the carbon flux due to the observed land-use changes.  
31  
32  
33 277 Houghton et al. (2012) estimated that the mean net carbon flux from land-use change  
34  
35  
36  
37 278 from 2000 to 2009 was a decrease of  $1.1 \text{ Pg C yr}^{-1}$ , and  $0.12 \text{ Pg C yr}^{-1}$  of this (about 10%)  
38  
39  
40  
41 279 was due to forest degradation. The annual global SR in 2009 decreased by  $1.0 \text{ Pg C yr}^{-1}$   
42  
43  
44 280 (from that in 2001, mainly due to decreased areas of woody savanna, deciduous broadleaf  
45  
46  
47  
48 281 forest and the cropland–natural vegetation mosaic. However, the previously reported  
49  
50  
51  
52 282 decrease in the area of evergreen broadleaf forest (mainly in tropical regions; Hansen et  
53  
54  
55 283 al., 2010; Keenan et al., 2015) could not be detected in the MODIS land cover map in the  
56  
57  
58  
59 284 present study. In addition, woody savanna and savanna were difficult to distinguish based  
60  
61  
62  
63  
64  
65

1  
2 285 on the MODIS data. We therefore need to do more work to develop MODIS products, and  
3  
4  
5 286 especially global land cover maps, at high spatial resolution that will let us better detect  
6  
7  
8  
9 287 land-use changes and evaluate the effects of these changes on the global carbon cycle.  
10

11  
12 288

13  
14  
15  
16 289 **5 Conclusions**  
17

18  
19 290 In the present study, we provided preliminary insights into the estimation of global  $R_s$  in  
20  
21  
22  
23 291 2001 and 2009 using empirically derived soil temperature equations for 17 ecosystems,  
24  
25  
26 292 climate data, and 4-km-resolution MODIS land-use maps. Land surface temperatures  
27  
28  
29 293 during the night ( $LST_n$ ) in the MODIS dataset were also important to estimate global  $R_s$ ,  
30  
31  
32  
33 294 as were daytime LST values ( $LST_d$ ) from winter to early summer in subarctic and  
34  
35  
36  
37 295 temperate ecosystems. The annual global  $R_s$  values did not differ greatly between 2001  
38  
39  
40 296 and 2009 (94.8 and 93.8 Pg C yr<sup>-1</sup>, respectively), but did suggest a slight decrease. The  
41  
42  
43  
44 297 decrease in annual global  $R_s$  in 2009 resulted mainly from decreased areas of woody  
45  
46  
47  
48 298 savanna, deciduous broadleaf forest, and the cropland–natural vegetation mosaic.  
49  
50  
51 299 However, due to the high uncertainties in the input data and equations used in our analysis,  
52  
53  
54  
55 300 it will be necessary to develop more accurate estimates of global  $R_s$  by (1) considering  
56  
57  
58  
59 301 other factors that affect  $R_s$  (e.g., age of vegetation, soil texture, SOC, and nitrogen  
60  
61  
62  
63  
64  
65

1  
2 302 fertilization) and (2) using global climate data and land-use maps obtained at higher

3  
4  
5  
6 303 spatial resolution.

7  
8  
9 304

10  
11  
12 305 Acknowledgements

13  
14  
15  
16 306 This research was supported by Green Network of Excellence project

17  
18  
19 307 (<http://grene.jp/english/>) and by the Ministry of Education, Culture, Sports, Science and

20  
21  
22  
23 308 Technology, Japan. This research was also supported by JSPS KAKENHI Grant Number

24  
25  
26 309 16H05787. We thank Dr A.W. Kishimoto-Mo of the National Institute for

27  
28  
29 310 Agro-Environmental Studies for providing the climate data from Tsukuba, Japan, and Dr

30  
31  
32  
33 311 M. Ueyama of Osaka Prefecture University, Dr H. Iwata of Shinshu University, and Dr Y.

34  
35  
36  
37 312 Harazono of the International Arctic Research Center, University of Alaska at Fairbanks,

38  
39  
40 313 for providing the climate data from Alaska. We also thank Dr T. Maeda of the National

41  
42  
43  
44 314 Institute of Advanced Industrial Science and Technology, Dr Y. Kosugi of Kyoto

45  
46  
47 315 University, and the researchers responsible for the AsiaFlux Database (<http://asiaflux.net>)

48  
49  
50  
51 316 for providing the climate data from Takayama (Japan), Sakaerat (Thailand), and Pasoh

52  
53  
54  
55 317 (Malaysia).

56  
57  
58 318

1  
2 **319 References**  
3

- 4 320 Beer, C., Reichstein, M., Tomelleri, E., Ciais, P., Jung, M., Carvalhais, N., Rödenbeck, C.,  
5  
6  
7 321 Arain, M.A., Baldocchi, D., Bonan, G.B., Bondeau, A., Cescatti, A., Lasslop, G.,  
8  
9  
10 322 Lindroth, A., Lomas, M., Luysaert, S., Margolis, H., Oleson, K.W., Rouspard, O.,  
11  
12 323 Veenendaal, E., Viovy, N., Williams, C., Woodward, F.I., Papale, D., 2010.  
13  
14  
15 324 Terrestrial gross carbon dioxide uptake: global distribution and covariation with  
16  
17 325 climate. *Science*. 329, 834–838.  
18  
19  
20 326 Bond-Lamberty, B.P., Thomson, A.M., 2010. Temperature-associated increases in the  
21  
22 327 global soil respiration record. *Nature*. 464, 579–583.  
23  
24  
25 328 Bond-Lamberty, B.P., Thomson, A.M., 2014. A Global Database of Soil Respiration Data,  
26  
27 329 Version 3.0. Data set, Available on-line from Oak Ridge National Laboratory  
28  
29 330 Distributed Active Archive Center, Oak Ridge, Tennessee, USA.  
30  
31 331 <http://daac.ornl.gov>(accessed 16.09.16).  
32  
33  
34  
35  
36 332 Carney, K.M., Hungate, B.A., Drake, B.G., Megonigal, J.P., 2007. Altered soil microbial  
37  
38 333 community at elevated CO<sub>2</sub> leads to loss of soil carbon. *P. Natl. Acad. Sci.* 104,  
39  
40 334 4990–4995.  
41  
42  
43  
44 335 Carvalhais, N., Forkel, M., Khomik, M., Bellarby, J., Jung, M., Migliavacca, M., Mu, M.,  
45  
46 336 Saatchi, S., Santoro, M., Thurner, M., Weber, U., Ahrens, B., Beer, C., Cescatti, A.,  
47  
48  
49 337 Randerson, J.T., Reichstein, M., 2014. Global covariation of carbon turnover times  
50  
51 338 with climate in terrestrial ecosystems. *Nature*. 514, 213–217.  
52  
53  
54 339 Chen, X., Eamus, D., Hutley L.B., 2002. Seasonal patterns of soil carbon dioxide efflux  
55  
56 340 from a wet-dry tropical savanna of northern Australia. *Aust. J. Bot.* 50, 43–51.  
57  
58  
59  
60  
61  
62  
63  
64  
65

- 1  
2 341 Davidson, E.A., Janssens, I.A., 2006. Temperature sensitivity of soil carbon  
3  
4 342 decomposition and feedbacks to climate change. *Nature*. 440, 165–173.  
5  
6  
7 343 Friedl, M.A., McIver, D.K., Hodges, J.C.F., Zhang, X.Y., Muchoney, D., Strahler, A.H.,  
8  
9 344 Woodcock, C.E., Gopal, S., Schneider, A., Cooper, A., Baccini, A., Gao, F., Schaaf,  
10  
11 345 C., 2002. Global land cover mapping from MODIS: algorithms and early results.  
12  
13 346 *Remote Sens. Environ.* 83, 287–302.  
14  
15  
16  
17 347 Guo, L.B., Gifford, R.M., 2002. Soil carbon stocks and land use change: a meta analysis.  
18  
19 348 *Glob. Change Biol.* 8, 345–360.  
20  
21  
22  
23 349 Guo, M., Wang, X., Li, J., Yi, K., Zhong, G., Tani, H., 2012. Assessment of global carbon  
24  
25 350 dioxide concentration using MODIS and GOSAT data. *Sensors*. 12, 16368–16389.  
26  
27  
28 351 Hansen, M.C., Stehman, S.V., and Potapov, P.V. 2010. Quantification of global gross  
29  
30 352 forest cover loss. *P. Natl. Acad. Sci.*, 107, 8650–8655, doi:  
31  
32 353 10.1073/pnas.0912668107.  
33  
34  
35  
36 354 Hashimoto, S., Carvalhais, N., Ito, A., Migliavacca, M., Nishina, K., Reichstein, M.,  
37  
38 355 2015. Global spatiotemporal distribution of soil respiration modeled using a global  
39  
40 356 database. *Biogeosciences*. 12, 4121–4132.  
41  
42  
43  
44 357 Hirano, T., Kusin, K., Limin, S., Osaki, M., 2014. Carbon dioxide emissions through  
45  
46 358 oxidative peat decomposition on a burnt tropical peatland. *Glob. Change Biol.* 20,  
47  
48 359 555–565.  
49  
50  
51  
52 360 Houghton, R.A., House, J.I., Pongratz, J., van der Werf, G.R., DeFries, R.S., Hansen,  
53  
54 361 M.C., Le Quéré, Ramankutty, N., 2012. Carbon emissions from land use and  
55  
56 362 land-cover change. *Biogeosciences*. 9, 5125–5142.  
57  
58  
59  
60  
61  
62  
63  
64  
65

1  
2 363 Ise, T., Litton, C.M., Giardina, C.P., Ito, A., 2010. Comparison of modeling approaches  
3  
4 364 for carbon partitioning: Impact on estimates of global net primary production and  
5  
6  
7 365 equilibrium biomass of woody vegetation from MODIS GPP. *J. Geophys. Res.* 115,  
8  
9 366 G04025.

10  
11  
12 367 Janssens, I.A., Dieleman, W., Luysaert, S., Subke, J-A., Reichstein, M., Ceulemans, R.,  
13  
14 368 Ciais, P., Dolman, A.J., Grace, J., Matteucci, G., Papale, D., Piaso, S.L., Schulze,  
15  
16  
17 369 E-D., Tang, J., Law, B.E., 2010. Reduction of forest soil respiration in response to  
18  
19 370 nitrogen deposition. *Nat. Geosci.* 3, 315–322.

20  
21  
22 371 Jiang, L., Shi, F., Li, B., Luo, Y., Chen, J., Chen, J., 2005. Separating rhizosphere  
23  
24 372 respiration from total soil respiration in two larch plantation in northeastern China.  
25  
26 373 *Tree Physiol.* 25, 1187–1195.

27  
28  
29 374 Kaufman, R.K., Kauppi, H., Mann, M.L., Stock, J.H., 2011. Reconciling anthropogenic  
30  
31 375 climate change with observed temperature 1998-2008. *P. Natl. Acad. Sci.* 108,  
32  
33 376 11790–11793.

34  
35  
36  
37  
38 377 Keenan, R.J., Reams, G.A., Achard, F., de Freitas, J.V., Grainger, A., Lindquis, E., 2015.  
39  
40 378 Dynamics of global forest area: Results from the FAO Global Forest Resources  
41  
42 379 Assessment 2015. *Forest Ecol. Manag.* 352, 9–20.

43  
44  
45  
46 380 Keetch, J.J., Byram, G.M., 1968. A drought index for forest fire contro, Res. Paper SE-38,  
47  
48 381 Asheville, NC: U.S. Department of Agriculture, Forest Service. Southeastern  
49  
50 382 Forest Experiment Station.

51  
52  
53 383 Kosaka, Y., Xie, S-P., 2013. Recent global-warming hiatus tied to equatorial Pacific  
54  
55 384 surface cooling. *Nature.* 501, 403–407.

56  
57  
58  
59  
60  
61  
62  
63  
64  
65

1  
2 385 Linderholm, H.W., 2006. Growing season changes in the last century. *Agr. Forest*  
3  
4 386 *Meteorol.* 137, 1–14.  
5  
6  
7 387 Mao, J., Thornton, P.E., Shi, X., Zhao, M., and Post, W.M., 2012. Remote sensing  
8  
9 388 evaluation of CLM4 GPP for the period 2000–09. *J. Climate.* 25, 5327–5342.  
10  
11  
12 389 Mo, W., Lee, M.S., Uchida, M., Inatomi, M., Saigusa N., Mariko, S., Koizumi, H., 2005.  
13  
14 390 Seasonal and annual variations in soil respiration in a cool-temperate deciduous  
15  
16 391 broad-leaved forest in Japan. *Agr. Forest Meteorol.* 134, 81–94.  
17  
18  
19 392 Post, W.M., Kwon, K.C., 2000. Soil carbon sequestration and land-use change: processes  
20  
21 393 and potential. *Glob. Change Biol.* 6, 317–327.  
22  
23  
24 394 Pypker, T.G., Fredeen, A.L., 2002. Ecosystem CO<sub>2</sub> flux over two growing seasons for a  
25  
26 395 sub-Boreal clearcut 5 and 6 years after harvest. *Agr. Forest Meteorol.* 114, 15–30.  
27  
28  
29 396 R Development Core Team: R, 2016. A language and environment for statistical  
30  
31 397 computing, R Foundation for Statistical Computing, Vienna, Austria, ISBN  
32  
33 398 3-900051-07-0, available at: <http://www.R-project.org/>  
34  
35  
36 399 Raich, J.W., Schelesinger, W.H., 1992. The global carbon dioxide flux in soil respiration  
37  
38 400 and its relationship to vegetation and climate. *Tellus.* 44B, 81–99.  
39  
40  
41 401 Reichstein, M., Beer, C., 2008. Soil respiration across scales: The importance of a  
42  
43 402 model-data integration framework for data interpretation. *J. Plant Nutr. Soil Sci.*  
44  
45 403 171, 344–354.  
46  
47  
48 404 Richards, A.E., Dathe, J., Cook, G.D., 2012. Fire interacts with season to influence soil  
49  
50 405 respiration in tropical savannas. *Soil Biol. Biochem.* 53, 90–98.  
51  
52  
53 406 Sasai, T., Ichii, K., Yamaguchi, Y., Nemani, R., 2005. Simulating terrestrial carbon fluxes  
54  
55  
56  
57  
58  
59  
60  
61  
62  
63  
64  
65

1  
2 407 using the new biosphere model “biosphere model integrating eco-physiological and  
3  
4 408 mechanistic approaches using satellite data” (BEAMS). *J. Geophys. Res.*, 10,  
5  
6 409 G02014.  
7  
8  
9 410 Sasai, T., Saigusa, N., Nasahara, K.N., Ito, A., Hashimoto, H., Nemani, R., Hirata, R.,  
10  
11 411 Ichii, K., Takagi, K., Sitoh, T.M., Ohta, T., Murakami, K., Yamaguchi, Y., and  
12  
13 412 Oikawa, T., 2011. Satellite-driven estimation of terrestrial carbon flux over far east  
14  
15 413 Asia with 1-km grid resolution. *Remote Sens. Environ.* 115, 1758–1771.  
16  
17  
18 414 Sato, H., Ito, A., Ito, A., Ise, T., Kato, E., 2015. Current status and future of land surface  
19  
20 415 models. *Soil Sci. Plant Nutr.* 61, 34–47.  
21  
22  
23 416 Saurette, D.D., Chang, S., Thomas, B.R., 2006. Some characteristics of soil respiration in  
24  
25 417 hybrid poplar plantations in northern Alberta. *Can. J. Soil Sci.* 86, 257–268.  
26  
27  
28 418 Smith, P., Fang, C., 2010. A warm response by soils. *Nature.* 464, 499–500.  
29  
30  
31 419 Sotta, E.D., Meir, P., Malhi, Y., Nobre, A.D., Hodnett, M., Grace, J., 2004. Soil CO<sub>2</sub>  
32  
33 420 efflux in a tropical forest in the central Amazon. *Glob. Change Biol.* 10, 601–617.  
34  
35  
36 421 Sugihara, S., Funakawa, S., Kilasara, M., Kosaki, T., 2012. Effects of land management  
37  
38 422 on CO<sub>2</sub> flux and soil C stock in two Tanzanian croplands with contrasting soil  
39  
40 423 texture. *Soil Biol. Biochem.* 46, 1–9.  
41  
42  
43 424 Takeuchi, W., Hirano, T., Anggraini, N., Roswintiarti, O., 2010. Estimation of ground  
44  
45 425 water table at forested peatland in Kalimantan using drought index towards wildfire  
46  
47 426 control, 31st Asian conference on remote sensing (ACRS): Hanoi, Vietnam.  
48  
49  
50 427 Takeuchi, W., Oyoshi, K., Akatsuka, S., 2012. Super-resolution of MTSAT land surface  
51  
52 428 temperature by blending MODIS and AVNIR2. *Asian Journal of Geoinformatics.*  
53  
54  
55  
56  
57  
58  
59  
60  
61  
62  
63  
64  
65

1  
2 429 12(2).  
3  
4 430 Ueyama, M., Iwata, H., Harazono, Y., 2014. Autumn warming reduces the CO<sub>2</sub> sink of a  
5  
6  
7 431 black spruce forest in interior Alaska based on a nine-year eddy covariance  
8  
9  
10 432 measurement. *Glob. Change Biol.* 20, 1161–1173.  
11  
12 433 Xia, J., Niu, S., Ciais, P., Janssens, I.A., Chen, J., Ammann, C., Arain, A., Blanken, P.D.,  
13  
14  
15 434 Cescatti, A., Bonal, D., Buchmann, N., Curtis, P.S., Chen, S., Dong, J., Flanagan,  
16  
17  
18 435 L.B., Frankenberg, C., Georgiadis, T., Gough, C.M., Hui, D., Kiely, G., Li, J., Lund,  
19  
20  
21 436 M., Mgliulo, V., Marcolla, B., Lutz, M., Montagnani, L., Moors, E.J., Olesen, J.E.,  
22  
23  
24 437 Piao, S., Raschi, A., Rouspard, O., Suyker, A.E., Urbaniak, M., Vaccari, F.P.,  
25  
26  
27 438 Varlagin, A., Vesala, T., Wikinson, M., Weng, E., Wohlfahrt, G., Yan, L., Luo, Y.,  
28  
29  
30 439 2015. Joint control of terrestrial gross primary productivity by plant phenology and  
31  
32  
33 440 physiology. *P. Natl. Acad. Sci.* 112, 2788–2793.  
34  
35  
36 441 Yokota, T., Yoshida, Y., Eguchi, N., Ota, Y., Tanaka, T., Watanabe, H. Maksyutov, S.,  
37  
38  
39 442 2009. Global concentrations of CO<sub>2</sub> and CH<sub>4</sub> retrieved from GOSAT: first  
40  
41  
42 443 preliminary results. *SOLA*, 5, 160-163.  
43  
44  
45 444 Yonemura, S., Nouchi, I., Nishimura, S., Sakurai, G., Togami, K., Yagi, K., 2014. Soil  
46  
47  
48 445 respiration, N<sub>2</sub>O and CH<sub>4</sub> emissions from an Andisol under conventional-tillage  
49  
50  
51 446 and no-tillage cultivation for 4 years. *Biol. Fert. Soils.* 50, 63–74.  
52  
53  
54 447 Yuan, W., Cai, W., Nguy-Robertson, A.L., Fang, H., Suyker, A.E., Chen, Y., Dong, W.,  
55  
56  
57 448 Liu, S., Zhang, H., 2015. Uncertainty in simulating gross primary production of  
58  
59  
60 449 cropland ecosystem from satellite-based models. *Agr. Forest Meteorol.* 207, 48-57.  
61  
62  
63 450 Zhou, T., Shi, P., Hui, D., Luo, Y., 2009. Global pattern of temperature sensitivity of soil  
64  
65

1  
2 451 heterotrophic respiration ( $Q_{10}$ ) and its implications for carbon-climate feedback. J.  
3  
4 452 Geophys. Res. 114, G02016.  
5  
6  
7 453  
8  
9 454  
10  
11  
12  
13  
14  
15  
16  
17  
18  
19  
20  
21  
22  
23  
24  
25  
26  
27  
28  
29  
30  
31  
32  
33  
34  
35  
36  
37  
38  
39  
40  
41  
42  
43  
44  
45  
46  
47  
48  
49  
50  
51  
52  
53  
54  
55  
56  
57  
58  
59  
60  
61  
62  
63  
64  
65

1  
2 **455 Figure legends**  
3

4 456 Figure 1. An overview of the estimation process for daily soil respiration at a global scale.  
5

6  
7 457 KBDI, Keetch–Byram drought index.  
8

9  
10 458  
11

12 459 Figure 2. Comparison between MODIS daytime and night surface temperatures ( $LST_d$   
13

14 and  $LST_n$ ), air temperature, and soil temperature and field observations in (a) an  
15

16  
17 461 evergreen needleleaf forest in Alaska, (b) a mixed forest in Japan, (c) cropland in Japan,  
18

19  
20 462 (d) an evergreen broadleaf forest in Thailand, and (e) an evergreen broadleaf forest in  
21

22  
23 463 Malaysia. The observation period and heights of air and soil temperatures differed among  
24

25  
26 464 the sites.  
27

28  
29 465  
30

31 466 Figure 3. The relationships between land surface temperature during the night ( $LST_n$ )  
32

33  
34 467 based on the MODIS dataset and soil temperature based on observation data from (a) an  
35

36  
37 468 evergreen needleleaf forest in Alaska (from March to April,  $LST_n > -12.0^\circ \text{C}$ ), (b) a  
38

39  
40 469 mixed forest in Japan (from April to July,  $LST_n > 6.5^\circ \text{C}$ ) and (c) cropland in Japan (from  
41

42  
43 470 January to July,  $LST_n > 0.0^\circ \text{C}$ ).  
44

45  
46 471  
47

48 472 Figure 4. Map of the global distribution of total annual soil respiration ( $R_s$ ) in (a) 2001  
49

50  
51 473 and (b) 2009.  
52

53  
54 474  
55

56 475 Figure 5. Mean annual soil respiration ( $R_s$ ) in the 17 ecosystems in 2001 and 2009. Table  
57

58  
59 476 S1 presents the  $R_s$  equations for each ecosystem type. Values are means  $\pm$  standard  
60  
61  
62  
63  
64  
65

1  
2  
3  
4  
5  
6  
7  
8  
9  
10  
11  
12  
13  
14  
15  
16  
17  
18  
19  
20  
21  
22  
23  
24  
25  
26  
27  
28  
29  
30  
31  
32  
33  
34  
35  
36  
37  
38  
39  
40  
41  
42  
43  
44  
45  
46  
47  
48  
49  
50  
51  
52  
53  
54  
55  
56  
57  
58  
59  
60  
61  
62  
63  
64  
65

477 deviations. None of the differences between 2001 and 2009 were statistically significant.

478 ENF, evergreen needleleaf forest; EBF, evergreen broadleaf forest; DNF, deciduous

479 needleleaf forest; DBF, deciduous broadleaf forest; MF, mixed forest; CS, closed

480 shrublands; OS, open shrubland; WS, woody savanna; SA, savanna; GL, grassland; PW,

481 permanent wetland; CL, cropland; UB, urban and build-up; CNV, cropland/natural

482 vegetation mosaic; SI, snow and Ice; BSV, barren or sparsely vegetation; TND, tundra.

483

484 Figure 6. Spatial variation in  $Q_{10}$  values estimated using the daily soil respiration ( $R_s$ )

485 values and MODIS land surface temperatures during the daytime ( $LST_d$ ).

486

Figure 1

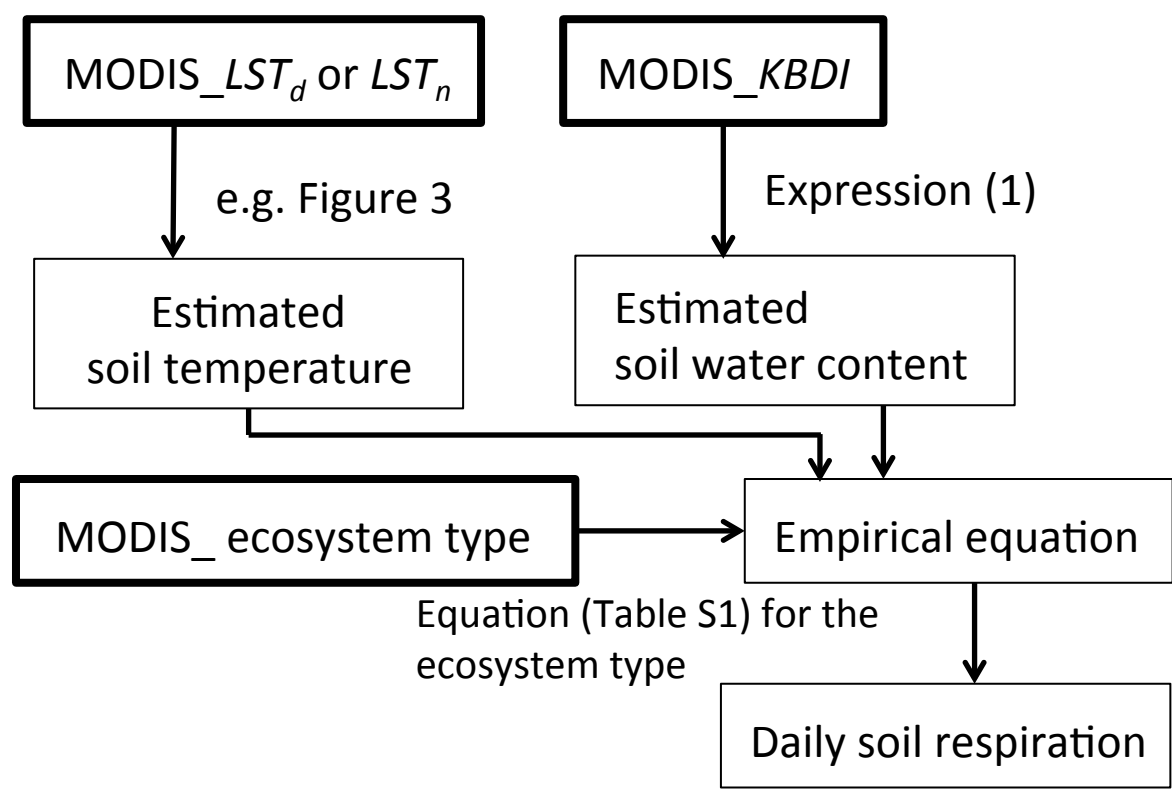


Figure 2

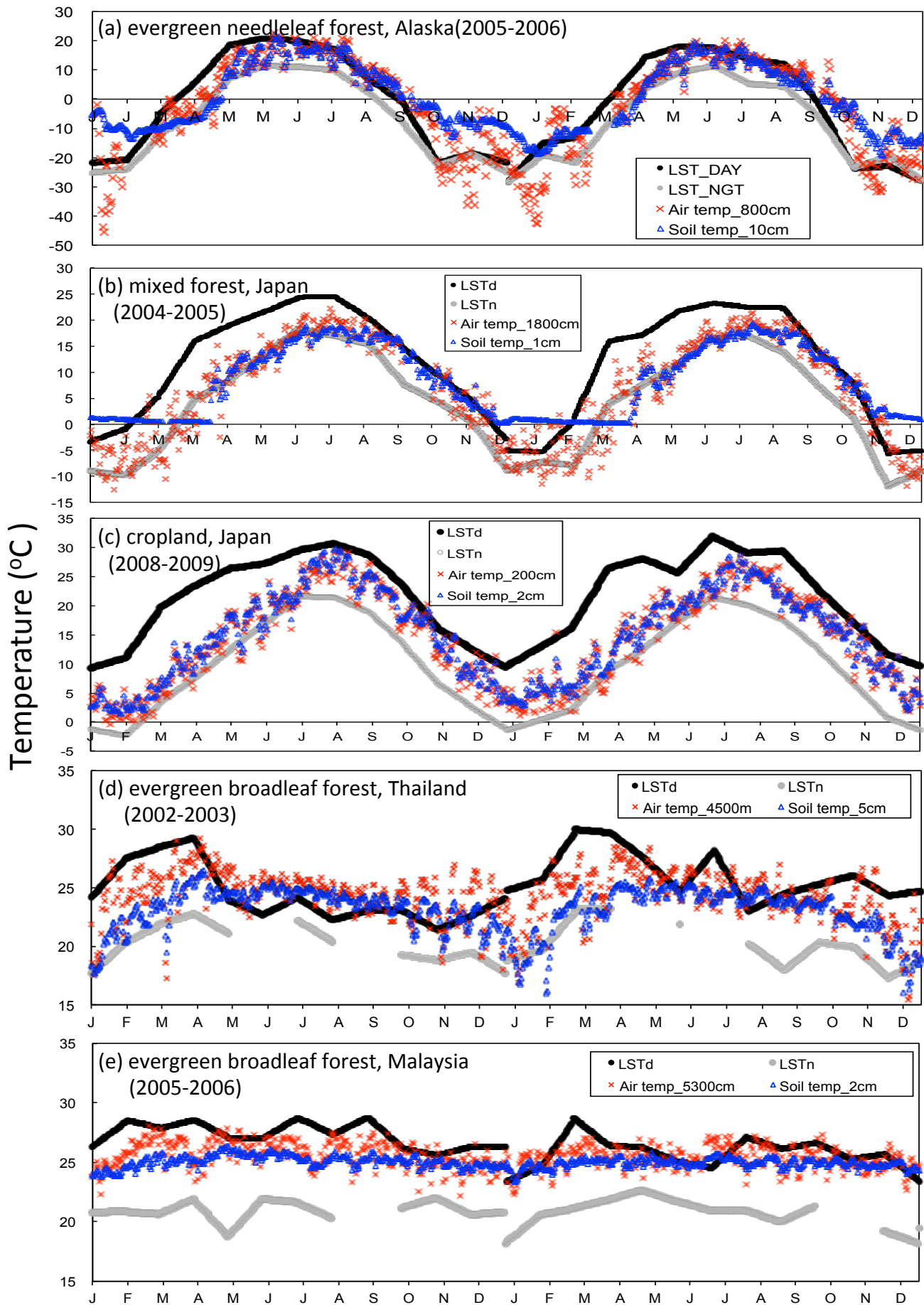


Figure 3

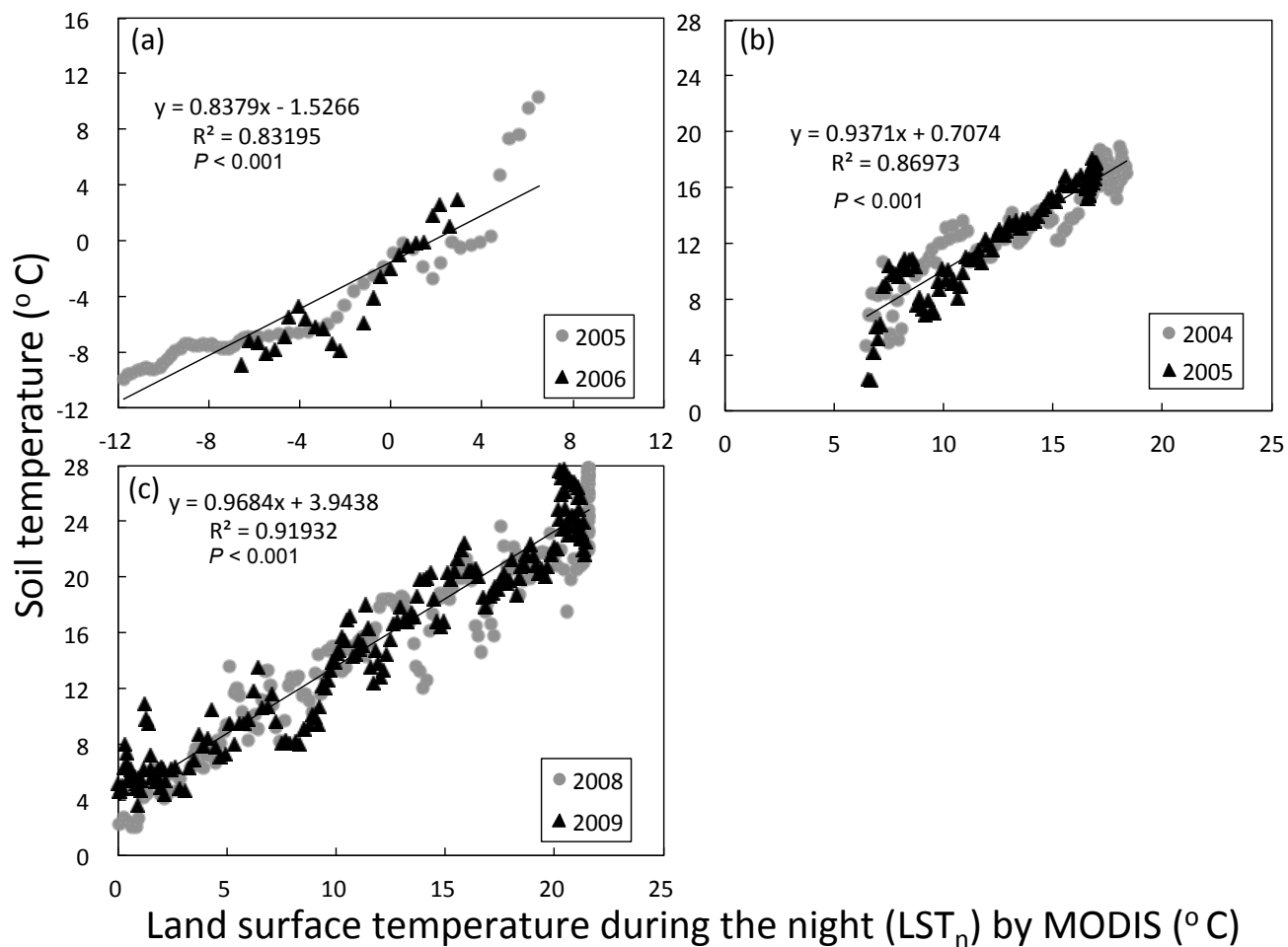


Figure 4

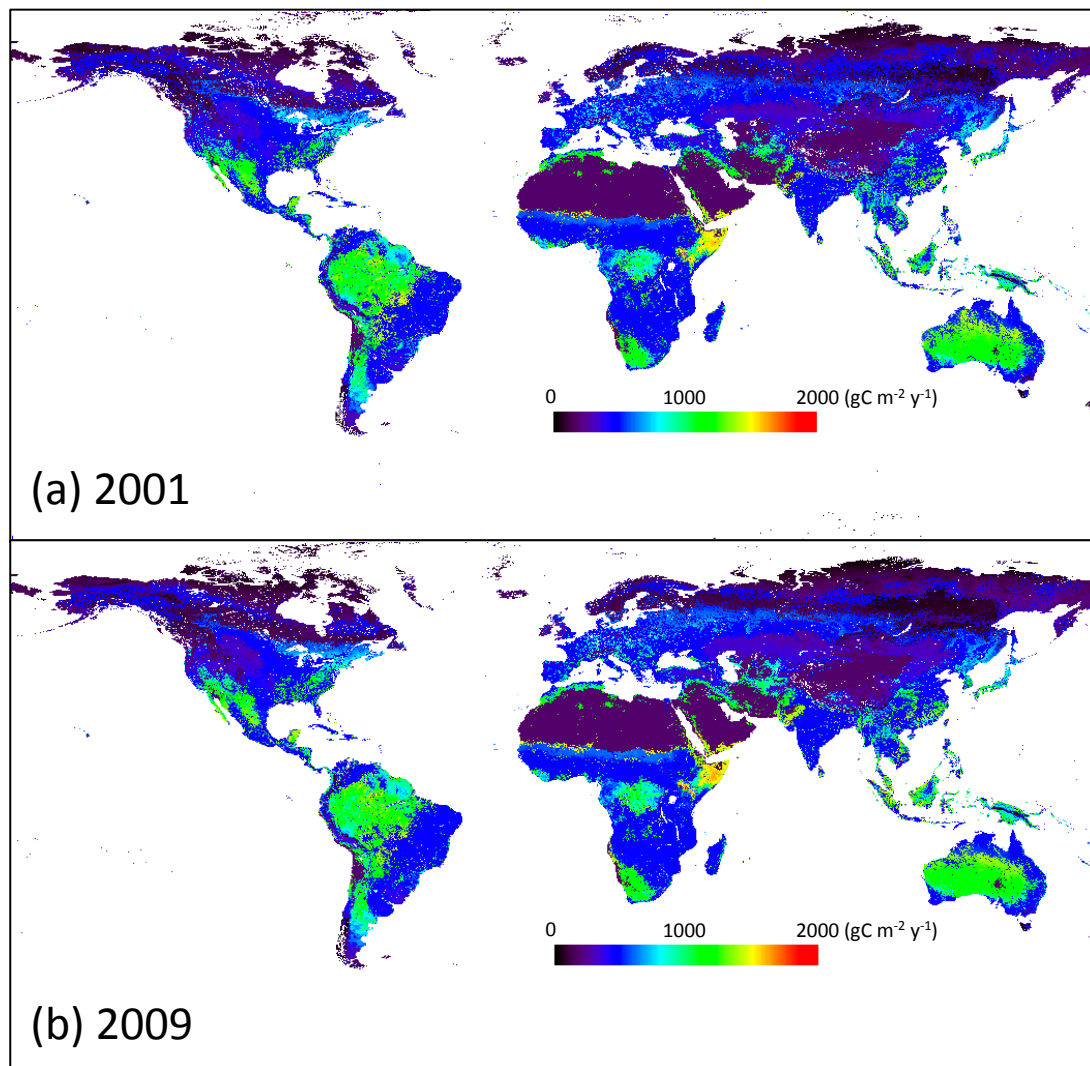


Figure 5

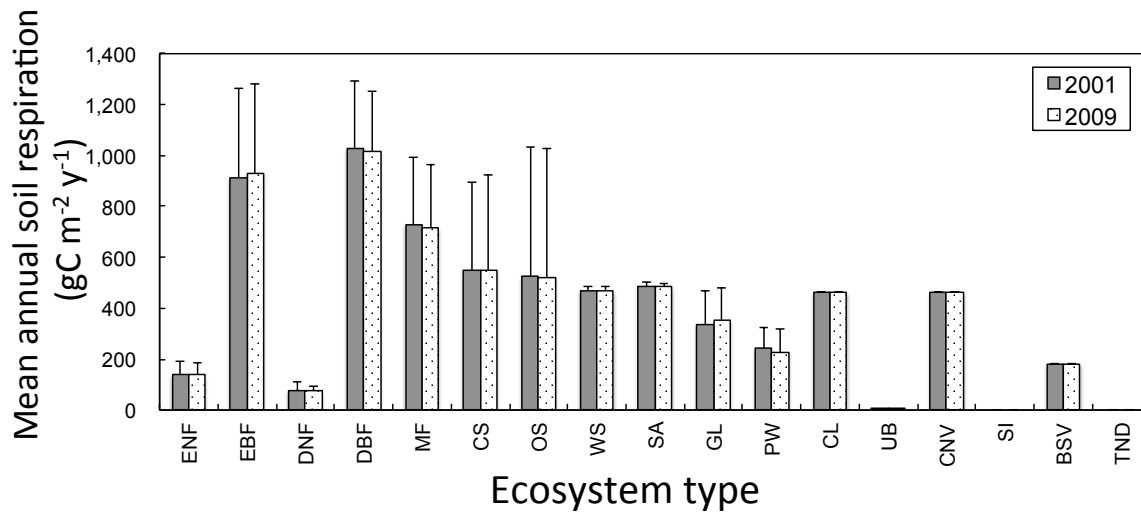


Figure 6

